

Time-resolved X-ray PIV technique for diagnosing opaque biofluid flow with insufficient X-ray fluxes

Sung Yong Jung,^{a,b} Han Wook Park,^{a,b} Bo Heum Kim^c and Sang Joon Lee^{a,b,c,d*}

Received 22 September 2012

Accepted 19 January 2013

^aDepartment of Mechanical Engineering, Pohang University of Science and Technology (POSTECH), San 31, Hyojadong, Pohang 790-784, Republic of Korea, ^bCenter for Biofluid and Biomimic Research, POSTECH, San 31, Hyojadong, Pohang 790-784, Republic of Korea, ^cGraduate School of Interdisciplinary Bioscience and Bioengineering, POSTECH, San 31, Hyojadong, Pohang 790-784, Republic of Korea, and ^dDivision of Integrative Biosciences and Biotechnology, POSTECH, San 31, Hyojadong, Pohang 790-784, Republic of Korea. E-mail: sjlee@postech.ac.kr

X-ray imaging is used to visualize the biofluid flow phenomena in a nondestructive manner. A technique currently used for quantitative visualization is X-ray particle image velocimetry (PIV). Although this technique provides a high spatial resolution (less than 10 μm), significant hemodynamic parameters are difficult to obtain under actual physiological conditions because of the limited temporal resolution of the technique, which in turn is due to the relatively long exposure time (~ 10 ms) involved in X-ray imaging. This study combines an image intensifier with a high-speed camera to reduce exposure time, thereby improving temporal resolution. The image intensifier amplifies light flux by emitting secondary electrons in the micro-channel plate. The increased incident light flux greatly reduces the exposure time (below 200 μs). The proposed X-ray PIV system was applied to high-speed blood flows in a tube, and the velocity field information was successfully obtained. The time-resolved X-ray PIV system can be employed to investigate blood flows at beamlines with insufficient X-ray fluxes under specific physiological conditions. This method facilitates understanding of the basic hemodynamic characteristics and pathological mechanism of cardiovascular diseases.

© 2013 International Union of Crystallography
Printed in Singapore – all rights reserved

Keywords: X-ray imaging; high-speed imaging; particle image velocimetry.

1. Introduction

Disorders in the circulatory vascular system are one of the main causes of mortality. Wall shear stress was recently identified as an important parameter in angiogenesis and cardiology, and a key player in cardiovascular diseases such as atherosclerosis (Malek *et al.*, 1999) and cardiogenesis (Hove *et al.*, 2003). *In vivo* measurement is essential for the hemorheological analysis of abnormal blood flows related to cardiovascular diseases. Noninvasive imaging techniques with a high spatial resolution are required to obtain detailed information on opaque blood flows in a circulatory vascular system.

In vivo experimental hemodynamic studies were performed using various medical imaging techniques, such as magnetic resonance imaging (MRI) (Bonn *et al.*, 2008; Canstein *et al.*, 2008) and echocardiography (Kheradvar *et al.*, 2010; Kim *et al.*, 2004; Niu *et al.*, 2010). Even though the three-dimensional velocity information of a blood flow can be measured using MRI, the MRI method cannot be used for *in vivo* blood flow analysis because of its insufficient spatial and temporal reso-

lution. Ultrasound imaging was combined with particle image velocimetry (PIV) to create the Echo PIV technique (Kim *et al.*, 2004), which implements a trade-off between the penetration depth and the spatial resolution of velocity field measurement. Therefore, Echo PIV and MRI both suffer from limited spatial resolution when used in diagnostic *in vivo* measurement of microscale biofluid flows.

The synchrotron X-ray imaging technique provides *in vivo* measurements with a high spatial resolution because of its advanced detection system and the penetration ability of its hard X-ray beam. As a result, this imaging technique was used to investigate biofluid flow phenomena in living organisms (Ahn *et al.*, 2010; Kim & Lee, 2010; Kim *et al.*, 2011; Lee & Kim, 2008; Lee & Lee, 2011; Westneat *et al.*, 2003). The X-ray PIV technique was developed to investigate blood flow at a high spatial resolution by combining the X-ray radiography and PIV velocity field measurement techniques (Lee & Kim, 2003, 2005a; Lee *et al.*, 2009). The X-ray PIV technique has been used to measure several types of liquids flowing inside opaque conduits (Im *et al.*, 2007; Kim & Lee, 2006; Lee & Kim, 2005b). This technique has recently advanced to the level

of three-dimensional velocity field measurement (Dubsky *et al.*, 2010, 2012; Fouras *et al.*, 2007; Irvine *et al.*, 2008, 2010; Jung & Lee, 2012; Lee *et al.*, 2011) and *in vivo* blood flow measurement (Jung *et al.*, 2012a).

Although the X-ray PIV system allows high spatial resolutions of less than 10 μm , important hemodynamic parameters, such as wall shear stress under a specific physiological condition, are difficult to obtain because of their limited temporal resolution. In X-ray fluoroscopy, image intensifiers have been used to intensify the fluorescence for easy observation (Krohmer, 1989). Recently, the image intensifier was employed in the X-ray PIV velocity field measurement (Jamison *et al.*, 2012). This previous work measured blood flows in a carotid artery. This *ex vivo* experiment was performed at the SPring-8 synchrotron which provides the highest X-ray flux in the world. The present study is focused on how to improve the temporal resolution of X-ray PIV measurements at beamlines

with insufficient X-ray fluxes. By adopting an image intensifier, we could overcome the low light efficiency of conventional lens-coupled image detection systems. In addition, it was verified that proper digital image processing methods are inevitable and useful to improve the image quality and to enhance measurement accuracy. The proposed X-ray PIV system was used to measure high-speed blood flow in a tube; thus, quantitative velocity field information was successfully obtained.

2. Time-resolved X-ray PIV system

The exposure time used for the image acquisition should be shortened to improve the temporal resolution of an X-ray imaging technique. The exposure time can be reduced by enhancing the photon flux of the illumination source or by using a high-performance imaging device. The first approach is practically impossible for individual researchers because upgrading a synchrotron light source is a long-term project and too expensive. Therefore, the second method of improving the temporal resolution was adopted in this study. An image intensifier was attached in front of a high-speed camera to amplify the incident light.

Fig. 1(a) shows how an image intensifier, which is a photosensitive vacuum tube, intensifies the incident light. Light is absorbed by the photocathode and causes electrons to be emitted into the vacuum. These electrons are accelerated by an electric field between the photocathode and the micro-channel plate (MCP), which is a thin plate consisting of approximately ten million parallel channels. The MCP voltage

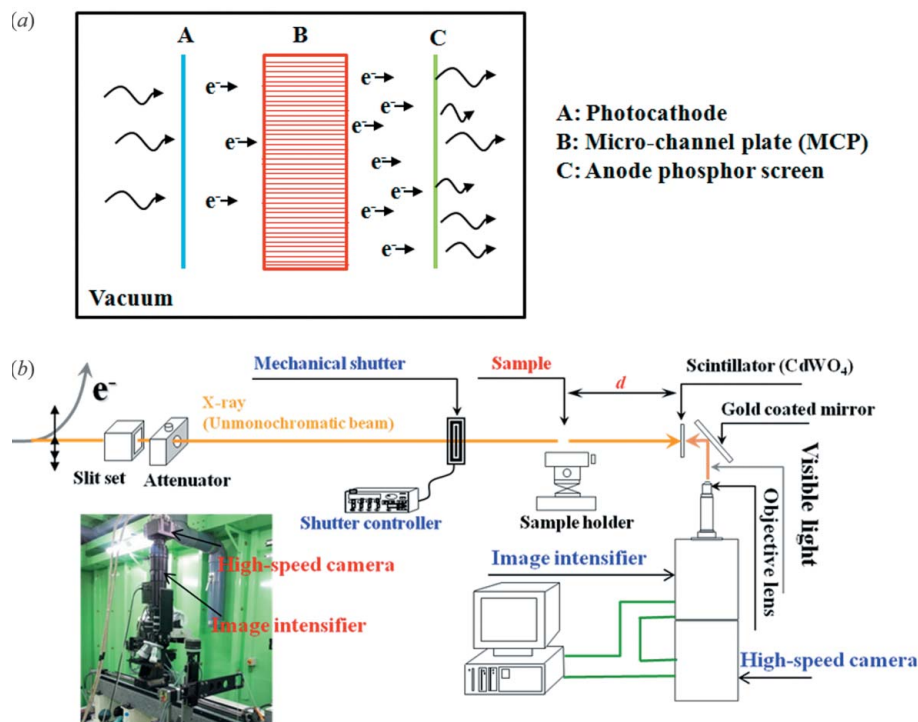


Figure 1 (a) Light intensification procedure in the image intensifier. (b) Schematic diagram of the time-resolved X-ray PIV system.

applied across the MCP creates an electric field inside each channel to accelerate the electrons. The electrons collide with the channel walls during their travel, which causes the emission of secondary electrons. This process of collision and emission of electrons is repeated many times in each channel, which results in the amplification of the number of electrons. The electrons leaving the MCP channels are accelerated by the electric field applied between the MCP and the anode screen. As electrons strike the anode screen, the energy of the electrons is converted back into light. Light intensity is greatly enhanced by this procedure, thereby dramatically reducing the image acquisition time. As a result, the temporal resolution of the X-ray imaging method is greatly improved.

A schematic diagram of the time-resolved X-ray PIV system is shown in Fig. 1(b). The experiment was carried out at 6D beamline of the Pohang Light Source (PLS-II, a third-generation synchrotron source) in South Korea. The maximum beam current and storage energy of the PLS-II are 400 mA and 3 GeV, respectively. A 100 mA beam current was used in this study. The unmonochromatic beam (white beam) with 1 mm-thick silicon as an attenuator had physical dimensions of 60 mm (horizontal) \times 5 mm (vertical). The energy bandwidth and corresponding median energy were 18.577 and 23.537 keV, respectively. The test samples were placed approximately 30 m downstream from the source, and the image detector (camera) was positioned 30 cm downstream from the sample. The size of the X-ray beam illuminating the test sample was adjusted to that of the field of view (FOV) by using a slit module to avoid accidental exposure of the sample to the X-ray beam. Aluminium sheets were placed at the beam

inlet of the experimental hutch in the pathway of the X-ray beam to attenuate the high-energy light flux, even when no X-ray image was acquired. In addition, a mechanical shutter only opened when an X-ray image was captured. Thus, the test sample and image detector were protected from being irradiated by the strong synchrotron X-ray beams.

An X-ray image of subnanometer wavelength was converted into a visible image by passing it through a thin CdWO₄ scintillator crystal. A gold-coated mirror reflects the visible image to avoid direct exposure of the camera to hard X-rays. The image was magnified with an objective lens and recorded by a high-speed complementary metal oxide semiconductor (CMOS) camera (Photron, FASTCAM ultima APX) at a resolution of 1024 × 1024 pixels. An image intensifier (Lambert Instrument, HiCATT) was positioned in front of the camera. The FOV with a 10× objective lens attached in front of the camera had approximate physical dimensions of 1.6 mm × 1.6 mm. X-ray images of the blood flow in an opaque silicon tube were consecutively captured.

3. Performance test of the time-resolved X-ray PIV system

The minimum exposure times required by the X-ray PIV system, with and without an image intensifier, to acquire an X-ray image of a resolution standard (X500-200-30; Xradia) were compared to evaluate the performance of the proposed X-ray PIV system. X-ray images of a living mosquito were also obtained, and the velocity field information of blood flow in an opaque silicon tube was measured using the proposed time-resolved X-ray PIV system.

3.1. Image processing to improve image quality

Raw X-ray images are of low contrast and exhibit granularity because of the short exposure time and the structural features of the image intensifier. Therefore, digital image processing is required to improve the quality of images before applying a PIV algorithm to the images. Flat-field correction, a type of background subtraction method, is commonly used to manipulate X-ray images (Jung *et al.*, 2012*b*). This method is useful for reducing the effects of the stationary structure of the image intensifier and the inhomogeneity of the X-ray beam. A median filter is also applied to reduce the noise and preserve the edges in the images. X-ray beam fluctuations caused by instabilities in the electron beam orbit of the synchrotron facility affect the acquired images because of the short exposure time. This negative effect can be overcome using a spatial-frequency filter. The image contrast is also enhanced to improve visibility by using the contrast-limited adaptive histogram equalization (CLAHE) algorithm, which partitions an image into contextual regions and applies the histogram equalization method to each region (Pisano *et al.*, 1998). Once the distribution of gray values is evened out, the hidden features of the image become more visible. The full gray spectrum is used to express the image in this process.

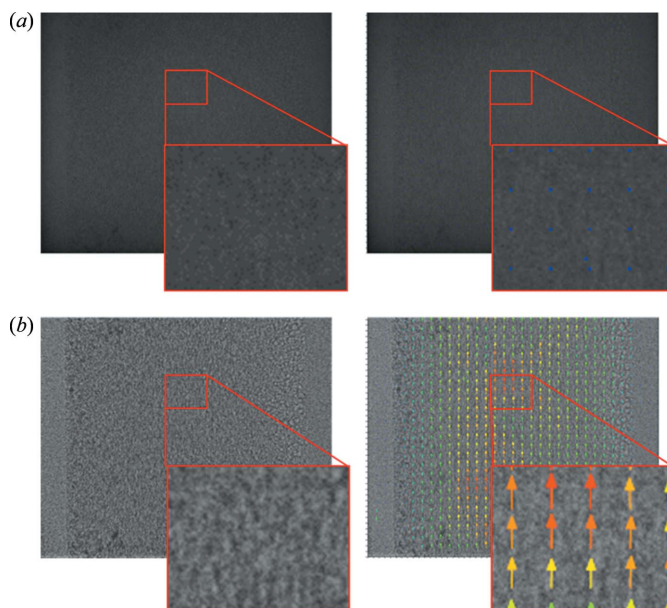


Figure 2
Comparison of the raw image (a) with the processed image (b). The left side shows images of whole blood flow seeded with silver-coated hollow glass particles in an opaque silicon tube, and the images on the right represent the instantaneous velocity vectors extracted from the left-side particle images.

Fig. 2 compares the processed image with its original raw image. The left side represents images of whole blood flow seeded with 14 μm silver-coated hollow glass particles in an opaque silicon tube with a diameter of 1500 μm. Compared with the raw image, the processed image exhibits significantly improved image contrast and signal-to-noise ratio (SNR). A cross-correlation PIV algorithm was applied to evaluate the digital image processing procedure. The resultant instantaneous velocity vectors are shown on the right side of Fig. 2. For the raw image, the peak position of the cross-correlation function used to obtain the displacement vectors of individual particles in the PIV analysis does not change, owing to the low SNR and poor image contrast. Therefore, inaccurate velocity information that identified the flow as almost stationary was obtained, although the motion of the flow was apparent in the consecutive flow images. By contrast, correct velocity information was successfully obtained from the processed images because of the high image contrast and good SNR. Digital image processing improves not only the image visibility but also the accuracy of PIV measurement.

3.2. Comparison of temporal resolution

The minimum exposure times with and without the image intensifier were compared to check the temporal resolution of the present X-ray imaging system. For this comparison, a resolution standard (X500-200-30; Xradia) was used as a stationary test object. Typical X-ray images captured with the minimum exposure time are shown in Fig. 3(a). Without the image intensifier, no recognizable image was obtained when the exposure time was shorter than 8 ms. Conversely, the minimum exposure time was reduced to 50 μs when the image

(a) Without intensifier ($t_{\text{exp}}=8\text{ ms}$) With intensifier ($t_{\text{exp}}=0.05\text{ ms}$)

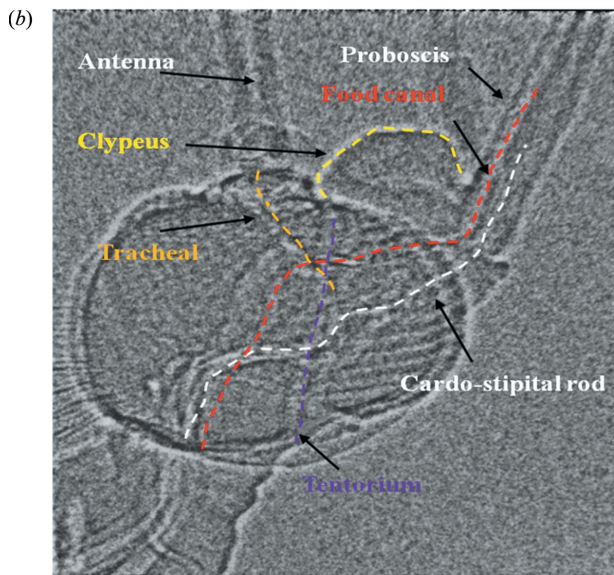
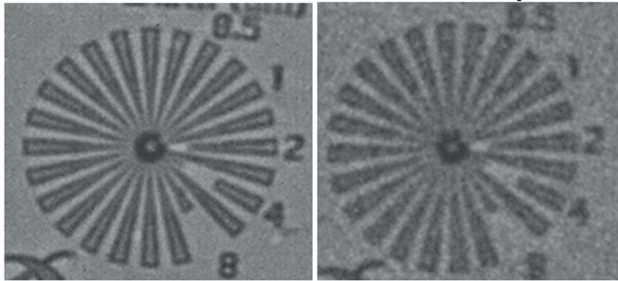


Figure 3
(a) Typical X-ray images of a resolution standard (X500-200-30; Xradia) captured at the minimum exposure time (t_{exp}) with and without the image intensifier. (b) X-ray image of the head of a living mosquito.

intensifier was used. Even though the image intensifier slightly increased the noise level of X-ray images, the standard test patterns are clearly visible. The X-ray imaging system proposed in this study greatly improved the temporal resolution with a reasonable spatial resolution of less than $5\ \mu\text{m}$. Therefore, the system can be used to measure hemodynamic parameters under a specific physiological condition.

An X-ray image of a living mosquito was also captured to verify the practical feasibility of the proposed X-ray PIV system for investigating the biofluid flow phenomena in living organisms. A typical X-ray image is shown in Fig. 3(b). The high-speed CMOS camera can record images at a full resolution of 1024×1024 pixels at 2000 frames per second (fps). Imaging at a higher frame rate is possible at a reduced resolution. Imaging feasibility was evaluated by varying the exposure time at a fixed frame rate of 2000 fps. The microscale morphological structures of the antenna, tracheal, clypeus, tentorium, proboscis, food canal and cardo-stipital rod inside the head of the mosquito were successfully observed at a minimum exposure time of $160\ \mu\text{s}$. The tracheal and cardo-stipital rods are closely related to the movements of the antenna and proboscis, respectively. Kim *et al.* (2011) investigated the overall sucking mechanism of a female mosquito by capturing consecutive X-ray images at 30 fps. A more

detailed sucking mechanism could be obtained if the X-ray images were captured in the same experiments at a much higher frame rate (shorter exposure time) by using the proposed system. This new X-ray imaging system shows a strong potential for use in diagnosing various biofluid flows in living organisms.

3.3. Velocity field measurement of whole blood flow

The proposed time-resolved X-ray PIV system was applied to measure the velocity fields of the flow of whole blood (40% Hematocrit) seeded with $14\ \mu\text{m}$ silver-coated hollow glass particles in an opaque silicon tube with a diameter of $1500\ \mu\text{m}$. The blood was supplied by a syringe pump at a flow rate of $2\ \text{ml min}^{-1}$. X-ray images were consecutively acquired at 2000 fps with an exposure time of $160\ \mu\text{s}$. The ratio of the exposure time to the time interval is important for improving the measurement accuracy (Fouras *et al.*, 2007); therefore, the present experimental condition with suitable digital image processing techniques improved the measurement accuracy. As shown in Fig. 2, the seeded tracer particles are apparent in the X-ray images, and no optical distortion occurred in the region near the tube wall. The quantitative instantaneous velocity field was obtained by applying a cross-correlation PIV algorithm to a pair of X-ray images. Fig. 4(a) illustrates the mean velocity field statistically obtained by ensemble averaging 200 instantaneous velocity fields. The mean velocity has a maximum value at the center of the tube, and has smaller values near the tube wall. The mean velocity field resembles the velocity field commonly observed in a fully developed flow inside a circular tube.

Fig. 4(b) shows a typical amassed velocity profile across the tube diameter, which was extracted from the mean velocity field in Fig. 4(a). The solid dots denote the experimental data obtained in this study, and the parabolic line represents the theoretical velocity profile. Based on the *in vitro* measurement of blood flows in our previous work (Kim & Lee, 2006), a potential region exists in which the velocity gradient is negligible because of the yield stress effect of the blood flow, even though the potential region is very small. In this study the blood cells were not directly visualized, and the velocity field was measured by seeding silver-coated hollow glass particles with a diameter of $14\ \mu\text{m}$ into the blood flow. The yield stress effect was not clearly observed at the center region of the tube due to technological limitation, even though whole blood was used as the working fluid.

For laminar flows in a circular tube installed vertically, the velocity profile can be evaluated using the Navier–Stokes equations and Poiseuille’s law,

$$U(r) = V_{\text{max}}[1 - (r/R)^2], \quad (1)$$

where R is the radius of the circular tube. Based on a previous study (Lee & Kim, 2003), the velocity information is amassed in X-ray PIV measurements. The amassed velocity profile is expressed as

$$U(r) = (2/3)V_{\text{max}}[1 - (x/R)^2], \quad (2)$$

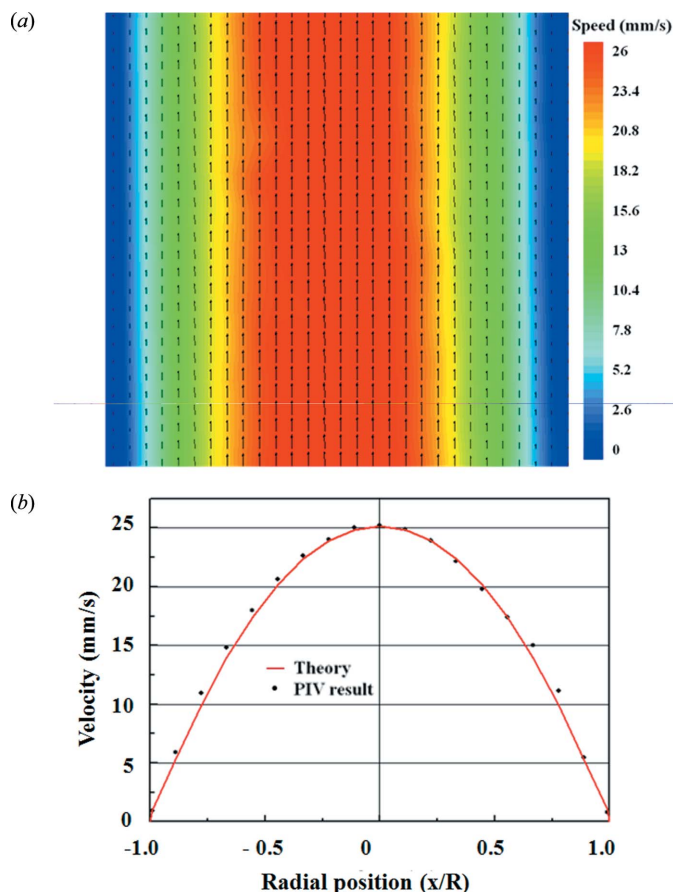


Figure 4
 (a) Mean velocity field of tracer particles seeded in the blood flow in a tube. (b) Comparison of the amassed velocity profiles.

where x is the radial position at the projection plane. The calculated theoretical flow rate based on the amassed velocity profile is about $2.073 \text{ ml min}^{-1}$. The experimental results measured with the time-resolved X-ray PIV system are in agreement with the theoretical results.

The difference in velocity is only approximately 3.67%. The maximum velocity at the tube center is approximately 25.21 mm s^{-1} , and the corresponding Reynolds number is 13.42 based on the following physical properties of the tested blood: a dynamic viscosity of $3 \times 10^{-3} \text{ kg m}^{-1} \text{ s}^{-1}$ and a blood density of 1065 kg m^{-3} . These values are significantly higher than the values in the previous study, wherein the maximum velocity and Reynolds number are approximately 0.5 mm s^{-1} and 0.49, respectively (Kim & Lee, 2006). Although the frame rate is fixed at 2000 fps to measure the velocity information of the entire tube at the highest spatial resolution of the high-speed camera used in the present study, the maximum measurable velocity can be increased by increasing the frame rate. The exposure time used in this experiment is $160 \mu\text{s}$, which results in a maximum possible frame rate of 6250 fps. This result implies that the measurable maximum velocity can be increased approximately three times by capturing X-ray images at a higher frame rate and at a reduced spatial resolution. However, the measurement accuracy will be slightly decreased because the ratio of exposure time to time interval

is increased (Fouras *et al.*, 2007). Given further supplementation, this new X-ray PIV system could be used to examine blood flows under actual physiological conditions.

4. Conclusion

A new time-resolved X-ray PIV system was proposed to investigate biofluid flow at beamlines with insufficient X-ray fluxes under certain physiological conditions. In this study an image intensifier was attached to a high-speed camera to reduce the exposure time and improve the temporal resolution of the X-ray imaging system. The incident light flux was amplified by emitting secondary electrons in the MCP of the image intensifier. The performance of the proposed system was evaluated by comparing the minimum exposure time required for image acquisition. Compared with the long exposure times used in previous research (approximately 10 ms), the exposure time in the proposed system is significantly reduced to less than $200 \mu\text{s}$. In addition, the new X-ray PIV system was applied to high-speed blood flow in a tube, and the velocity field information was successfully obtained after proper digital image processing. The time-resolved X-ray PIV system could be used to investigate blood flow under actual physiological conditions in the near future. Eventually, this system will greatly contribute to the hemodynamic and pathological analysis of cardiovascular diseases and clinical diagnosis.

This work was supported by the Creative Research Initiatives (Diagnosis of Biofluid Flow Phenomena and Biomimic Research) and the World Class University program through the National Research Foundation of Korea funded by the Ministry of Education, Science and Technology (R31-2008-000-10105-0). The authors are grateful for the valuable help in the X-ray imaging experiments performed at the 6D beamlines of the Pohang Accelerator Laboratory (Pohang, Korea).

References

Ahn, S., Jung, S. Y., Lee, J. P., Kim, H. K. & Lee, S. J. (2010). *ACS Nano*, **4**, 3753–3762.
 Bonn, D., Rodts, S., Groeninck, M., Rafai, S., Shahidzadeh-Bonn, N. & Coussot, P. (2008). *Annu. Rev. Fluid Mech.* **40**, 209–233.
 Canstein, C., Cachot, P., Faust, A., Stalder, A. F., Bock, J., Frydrychowicz, A., Küffer, J., Hennig, J. & Markl, M. (2008). *Magn. Reson. Med.* **59**, 535–546.
 Dubsky, S., Jamison, R. A., Higgins, S. P. A., Siu, K. K. W., Hourigan, K. & Fouras, A. (2012). *Exp. Fluids*, **52**, 543–554.
 Dubsky, S., Jamison, R. A., Irvine, S. C., Siu, K. K. W., Hourigan, K. & Fouras, A. (2010). *Appl. Phys. Lett.* **96**, 023720.
 Fouras, A., Dusting, J., Lewis, R. & Hourigan, K. (2007). *J. Appl. Phys.* **102**, 064916.
 Hove, J. R., Köster, R. W., Forouhar, A. S., Acevedo-Bolton, G., Fraser, S. E. & Gharib, M. (2003). *Nature (London)*, **421**, 172–177.
 Im, K., Fezzaa, K., Wang, Y. J., Liu, X., Wang, J. & Lai, M. (2007). *Appl. Phys. Lett.* **90**, 091919.
 Irvine, S. C., Paganin, D. M., Dubsky, S., Lewis, R. A. & Fouras, A. (2008). *Appl. Phys. Lett.* **93**, 153901.

- Irvine, S. C., Paganin, D. M., Jamison, A., Dubsky, S. & Fouras, A. (2010). *Opt. Express*, **18**, 2368–2379.
- Jamison, R. A., Siu, K. K. W., Dubsky, S., Armitage, J. A. & Fouras, A. (2012). *J. Synchrotron Rad.* **19**, 1050–1055.
- Jung, S. Y., Ahn, S., Nam, K. H., Lee, J. P. & Lee, S. J. (2012a). *Int. J. Cardiovasc. Imaging*, **28**, 1853–1858.
- Jung, S. Y. & Lee, S. J. (2012). *Rev. Sci. Instrum.* **83**, 046102.
- Jung, S. Y., Lim, S. & Lee, S. J. (2012b). *J. Hydrol.* **452**, 83–89.
- Kheradvar, A., Houle, H., Pedrizzetti, G., Tonti, G., Belcik, T., Ashraf, M., Lindner, J. R., Gharib, M. & Sahn, D. (2010). *J. Am. Soc. Echocardiogr.* **23**, 86–94.
- Kim, B. H., Kim, H. K. & Lee, S. J. (2011). *J. Exp. Biol.* **214**, 1163–1169.
- Kim, G. B. & Lee, S. J. (2006). *Exp. Fluids*, **41**, 195–200.
- Kim, H. B., Hertzberg, J. R. & Shandas, R. (2004). *Exp. Fluids*, **36**, 455–462.
- Kim, H. K. & Lee, S. J. (2010). *New Phytol.* **188**, 1085–1098.
- Krohmer, J. S. (1989). *Radiographics*, **9**, 1129–1153.
- Lee, W.-K., Fezzaa, K. & Uemura, T. (2011). *J. Synchrotron Rad.* **18**, 302–304.
- Lee, S. & Kim, G. (2003). *J. Appl. Phys.* **94**, 3620.
- Lee, S. J. & Kim, G. B. (2005a). *J. Appl. Phys.* **97**, 064701.
- Lee, S. J. & Kim, S. (2005b). *Exp. Fluids*, **39**, 492–497.
- Lee, S. J. & Kim, Y. (2008). *Ann. Bot.* **101**, 595–602.
- Lee, S. J., Kim, G. B., Yim, D. H. & Jung, S. Y. (2009). *Rev. Sci. Instrum.* **80**, 033706.
- Lee, S. J. & Lee, J. P. (2011). *Microsc. Res. Tech.* **74**, 517–522.
- Malek, A., Alper, S. & Izumo, S. (1999). *J. Am. Med. Assoc.* **282**, 2035–2042.
- Niu, L., Qian, M., Wan, K., Yu, W., Jin, Q., Ling, T., Gao, S. & Zheng, H. (2010). *Phys. Med. Biol.* **55**, 2103–2120.
- Pisano, E. D., Zong, S., Hemminger, B. M., DeLuca, M., Johnston, R. E., Muller, K., Braeuning, M. P. & Pizer, S. M. (1998). *J. Digit. Imaging*, **11**, 193–200.
- Westneat, M. W., Betz, O., Blob, R. W., Fezzaa, K., Cooper, W. J. & Lee, W. K. (2003). *Science*, **299**, 558–560.